Automated 3D registration of Magnetic Resonance Angiography, 3D Power Doppler, and 3D B-mode ultrasound images of carotid bifurcation

Piotr J. Slomka[*abc], Jonathan Mandel[c], Aaron Fenster[abc] and Donal Downey[ac]
[a]Diagnostic Radiology and Nuclear Medicine, London Health Sciences Centre,
London, Ontario, Canada, N6A 4G5
[b]Medical Biophysics, University of Western Ontario, London, Ontario, Canada
[c]Imaging Research Laboratory, John P. Robarts Research Institute, London, Ontario, Canada.

ABSTRACT

To allow a more objective interpretation of 3D carotid bifurcation images, we have implemented and evaluated on patient data, automated volume registration of 3D magnetic resonance angiography (MRA), 3D power Doppler (PD) ultrasound, and 3D B-mode ultrasound.

Our algorithm maximizes the mutual information between the thresholded intensities of the MRA and PD images. The B-mode images, acquired simultaneously in the same orientation as PD, are registered to the MRA using the transformation obtained from the MRA-PD registration. To test the algorithm we misaligned clinical ultrasound images and simulated mismatches between the datasets due to different appearances of diseased vessels by removing 3D sections of voxels from each of the paired scans. All registrations were assessed visually using integrated 3D volume, surface, and 2D slice display. 97% of images misaligned within a range of 40° and 40 pixels were correctly registered. The deviation from the mean registration parameters due to the simulated defects was 1.6±2.5°, 1.5±1.6 pixels in X ,Y and 0.7±0.7 pixels in Z direction. The algorithm can be used to register carotid images with misalignment range of 40 pixels in X, Y directions, 10 pixels in Z direction and 40° rotations, even in the case of different image appearances due to vessel stenoses.

Keywords: Image registration, ultrasound, magnetic resonance angiography

1. INTRODUCTION

As three dimensional (3D) clinical imaging techniques become increasingly ubiquitous, the need to evaluate the efficacy of these techniques becomes important. Currently there are several 3D techniques available for scanning of the carotid bifurcation. Two non-invasive techniques are magnetic resonance angiography (MRA) and 3D ultrasound. As of yet, a comparison of the diagnostic abilities of 3D ultrasound and MRA has not been performed for imaging the carotid bifurcation. In order to determine the future value these techniques, it is desirable to quantitatively compare the diagnostic abilities of MRA and 3D ultrasound. Such a comparison would involve assessment of both modalities in depicting the anatomy and lesions of the carotid bifurcation at the same locations in both images, and correlating the images with subsequent clinical events. For example, MRA and 3D ultrasound each have specific limitations in diagnosing carotid disease. Stenoses with reverse flow, such as turbulence, are invisible in MRA. Stenoses with calcified plaques are usually difficult to analyze with 3D ultrasound. Whereas each technique separately has shortcomings in imaging the carotid bifurcation, perhaps the fusion of the two modalities might overcome these limitations and aid clinical diagnosis.

The 3D algorithms and techniques for multimodality image fusion have been well explored for the coregistration of MRI, CT, PET and SPECT brain images[1-4]. However, the multimodality image registration of other organs has been investigated to a lesser extent. Semi-automated image registration techniques have been applied to cardiac[5,6] and thorax images[7]. The registration techniques can be divided into landmark-based, which require a set of fiducial markers, and image-based, which

[*] Corresponding author: e-mail: pslomka@irus.rri.on.ca; WWW: www.irus.rri.on.ca/~pslomka;
Fax: 1-519-667-6734

use intrinsic image features to estimate the correct spatial transformation between two 3D volumes. In many cases the position of the fiducial markers is already associated with significant errors and therefore the registration techniques based on intrinsic image features are preferred[8]. Often there is no merit in using external markers, due to the non-rigid character of the organs, or internal displacements. This is true in the case carotid arteries where the use of markers is not feasible. Thus, a preferred method of automatic registration of carotid vessel images should be based on image features. To our knowledge such automated registration techniques have not been developed to register 3D ultrasound of carotid vessels to other modalities. The difficulties in registering these data include the limited field of view of imaged organs and the noisy character of ultrasound images.

The aim of this study was to overcome these difficulties and to develop a tool for integration of 3D Power Doppler and 3D B-mode ultrasound images with MRA images. To investigate the performance of the algorithm we have quantitatively evaluated the acceptable range of the initial misalignments, as well as the effect of the differences in appearance of abnormal vessels in either modality. These tests were applied to a pilot set of clinical data.

2. METHODS

2.1 Image acquisition and patient data

Six patients undergoing conventional angiography for assessment of the carotid bifurcation were included in the study. The patients were imaged with the following modalities: 3D magnetic resonance angiography (MRA), 3D PD ultrasound, and 3D B-mode ultrasound. Thus one dataset for each patient consisted of three separate volumes of data.

The 3D MRA was performed on a GE Signa MR imaging system with either a 0.5 Tesla, or 1.5 Tesla field strength (General Electric, Milwaukee, Wisconsin). The acquisition parameters for the 0.5 Tesla images were TR 42 msec, TE 5.7 msec, bandwidth 9.14 kHz, FOV 20x15cm, matrix size 256x160, using a ramped RF pulse, 45° flip angle. The parameters for the 1.5 Tesla images were TR 34 msec, TE 5.1 msec, bandwidth 16 kHz, FOV 20x15cm, matrix size 256x160, with a ramped RF pulse, 45° flip. The pixel size was 0.13mmx0.13mmx1mm. All images were scanned with the Multiple Overlapping Thin Slab Acquisition (MOTSA) technique [9].

The 3D ultrasound images were acquired using a freehand 3D ultrasound system developed in our laboratory[10,11], which was coupled to an Ultramark 9 HDI Ultrasound System (ATL, Bothell, Washington). The images were acquired at a transducer frequency of 7 MHz. The freehand system used a six degree-of-freedom magnetic field sensor (Flock-of-Birds, Ascension Technology Corporation, Burlington, Vermont) to track the ultrasound transducer's position and orientation. The device consists of a magnetic field transmitter placed close to the patient and a receiver mounted on the transducer. By measuring the local magnetic field, the position and angulation of the receiver relative to the transmitter was determined. At the time of acquisition, electromagnetic interference was minimized and ferrous and highly conductive metals were absent from the vicinity. Individual 2D images were acquired with the transducer's position and orientation at a frame rate of 7 Hz, and were then reconstructed into a Cartesian 3D volume, then reformatted to match the MRA pixel size. The 2D B-mode and power Doppler images were acquired at the same time through separate data channels from the Ultramark 9 system, resulting in geometrically registered 3D B-mode and 3-D power Doppler images.

2.2 Image Registration

We have implemented a voxel-based algorithm, which iteratively adjusts a set of 3 rotational and 3 translational parameters of the 3D Power Doppler ultrasound volume to align it with the MRA volume. Since the original ultrasound volumes have been acquired in various orientations differing up to 180º from the MRA orientation, we applied initial interactive reorientation of ultrasound to an approximate position of MRA (+-20 pixels, +-40º). This step could be automated if the approximate orientation of the ultrasound acquisition was recorded with the data. All subsequent steps were fully automated. The simplex based optimization algorithm[12] minimized the cost function defining the quality of alignment between the MRA and transformed PD ultrasound images. PD ultrasound images were transformed using tri-linear interpolation. A simplex algorithm independently adjusted six transformation parameters: X shift, Y shift, Z shift, XY tilt, XZ tilt, and YZ tilt. [3]Since the pixel sizes were known and appropriately adjusted before the registrations, the scaling in X,Y, and Z were constrained. The cost function used was based on the mutual information function of two registered volumes[13]. The iteration process was terminated when the relative increase in the mutual information value was below a predefined threshold for all transformations in one simplex cycle. The 3D B-mode ultrasound images, acquired simultaneously and in the same orientation as PD images, were then transformed and superimposed on the MRA images using the transformation parameters obtained from the automatic MRA-PD registration.

Mutual information theory[13] defines the measure of the degree of dependence of one random variable on another. Its application has been previously shown to be successful in registration of MRI, CT, and PET images of the brain[1-3]. Assuming that the highest degree of dependence between the image data occurs when the data are properly aligned, we can seek to maximize the mutual information as a function of transformation parameters. If *U* (transformed ultrasound) and *M* (MRA) data are defined as two random variables and have two marginal probability distributions $p_U(u)$ and $p_M(m)$ and a joint probability distribution $p_{UM}(u,m)$, then the mutual information between *U* and *M*, MI(*U,M*) is given as:

$$MI(U,M) = \sum_{u,m} p_{UM}(u,m) \log \frac{p_{UM}(u,m)}{p_U(u) * p_M(m)} \quad (1)$$

The $p_{UM}(u,m)$ is defined as the number of voxels with intensities *u* on Ultrasound and *m* on MRA, divided by the number of all voxels in the volume:

$$p_{UM}(u,m) = \frac{\#(\{(x,y,z) \mid U(x,y,z) = u \text{ and } M(x,y,z) = m\})}{X * Y * Z} \quad (2)$$

where, the X, Y,Z are the 3-D dimensions of the volumes and x,y,z individual voxel locations. Subsequently, the $p_U(u)$ and $p_M(m)$ are derived as:

$$p_U(u) = \sum_m p_{UM}(u,m)$$
$$p_M(m) = \sum_u p_{UM}(u,m) \quad (3\text{-}4)$$

2.3 Multimodal image visualization and visual verification of the results

The image visualization has been performed on a medical imaging workstation (HERMES, Nuclear Diagnostics, Stockholm, Sweden). The result of each automated alignment was assessed visually on all image slices in different orientations simultaneously, using interactive 3D display (Figure 1). Please see the web site (http://www.irus.rri.on.ca/~pslomka/usmra) for color images and other patient cases.

Figure 1. Assessment of the alignment in an interactive 3D display. Image on the left represents the MRA, on the right, 3D Power Doppler Ultrasound overlaid on MRA in a different shade (different color scheme on the computer monitor).

Several visual presentation techniques were used to verify the registered image accuracy: a roving window display technique, 2D and 3D image overlay of the registered image with the baseline image. A composite 3D shear warp volume rendering technique[14] was used for the integrated 3D visualization of the MRA and ultrasound data. The registered images were qualitatively judged by the observer as correctly aligned, satisfactorily aligned, or poorly aligned.

2.4 Registration reproducibility test

In order to determine the effect of the initial misalignment of the data on the registration algorithm and the effective range of transformation parameters which can be successfully adjusted by the registration, we tested the registration performance after gradually varying misalignment of the ultrasound data in different directions and different orientations. We varied the misalignment of angles from 0 to 90°, the translation misalignment from 0 to 80 pixels in X and Y direction, and 0 to 40 pixels in Z direction (long axis of the vessels). We measured quantitatively the effect of the initial misalignment on the registration quality by defining the total 3D displacement error caused by the differences of the transformation parameters[7]. This error was calculated from an average of 4 different anatomical locations in the image (apex of the carotid bifurcation, selected points in internal, external, and common carotids. The displacement d was defined as a 3-D distance between points transformed according to the true transform T_t, (defined as the average transform for all successful registrations) and the actual transform T . Due to the errors in the shifts and angles, the point P can be transformed into point P' or P'' with homogeneous co-ordinates (x_h', y_h', z_h', w') or $(x_h'', y_h'', z_h'', w'')$:

.

$$\begin{bmatrix} x_h' \\ y_h' \\ z_h' \\ w' \end{bmatrix} = T \begin{bmatrix} x_h \\ y_h \\ z_h \\ w \end{bmatrix}, \quad \begin{bmatrix} x_h'' \\ y_h'' \\ z_h'' \\ w'' \end{bmatrix} = T_t \begin{bmatrix} x_h \\ y_h \\ z_h \\ w \end{bmatrix} \quad (5)$$

The 3-D displacement in mm (d) corresponding to this transformation, is expressed as:

$$d = \sqrt{(x' - x'')^2 + (y' - y'')^2 + (z' - z'')^2} \quad (6)$$

Thus the total average, and maximum displacement registration error (TDRE) was defined as

$$\overline{TDRE_m} = \frac{\sum_n d_{nm}}{n}, \quad TDRE\max_m = \max_n(d_{nm}) \quad (7)$$

Where n is the index of the patient's dataset, and m is the index of each misalignment.

2.5 Simulated defect tests

We also tested the effect of missing data in each volume on the registration quality. In this experiment we simulated a poor appearance of the vessel in the image by removing a segment of the vessel. Such poor appearance could be caused by stenosis or image artifacts visible in one of the modalities. Since the long axis of the vessels was approximately aligned with the Z axis of the matrix, we varied the size of such segments by selecting a number of image slices, and subsequently setting to 0, all voxels inside the cross-sections of the vessel, within a given slice range (Figure 2).

Such defects were created on MRA images as well as on ultrasound images. Defects were created in different regions of the images: internal artery - region1, external artery - region2, a sum of both arteries - region3. The size of the defects was varied by extending the range of the 3D regions from 4 to 12 slices. The ultrasound images were then misaligned and the registration process was repeated. The Simulated Defect Registration Error (SDRE) due to such differences in image appearance was defined as a mean and maximum of absolute differences from the "gold standard" for each registration parameter. The “gold standard” of the transformation parameters for a given patient was defined, to be the mean transformation of all registrations, which have been visually assessed as correct for that patient, without presence of artificial defects. The formula describing the mean and maximum SDRE error is given in the equations below

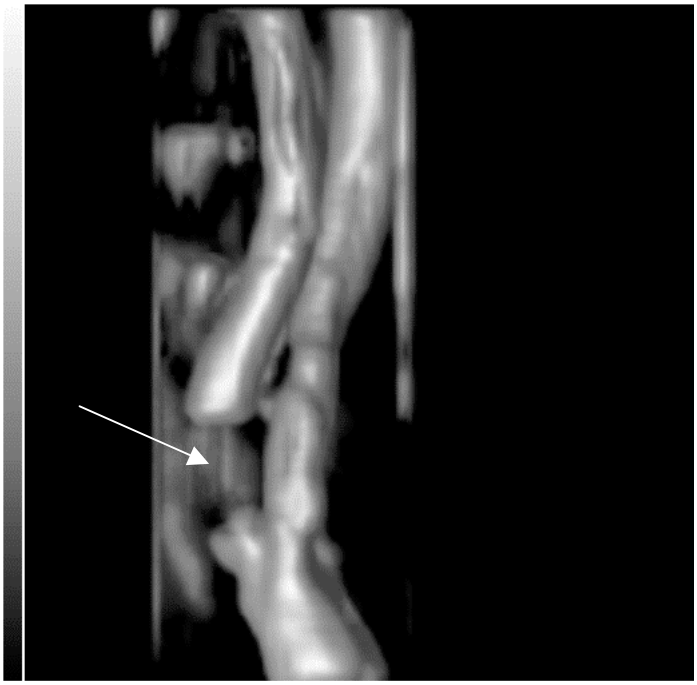

Figure 2. An example of a simulated defect. The arrow on the image points to the area where a segment of the artery was removed in order to simulate image mismatch due to vessel stenosis

$$\overline{SDRE}_{is} = \frac{\sum_{k}\sum_{n}\left|t_{iknS} - tt_{in}\right|}{kn} \qquad (8)$$

$$max(\mathrm{SDRE}_{is}) = \max_{kn}(\left|t_{ikn} - tt_{in}\right|) \qquad (9)$$

Where t_i is the one of 6 transformation parameters (i=1 to 6), tt_i is the true value for that parameter, k is the index of the location of simulated defects in either ultrasound or MRA, n is the index of the patient's dataset, s is the index of the varying defect size. These errors were calculated for each defect size and each transformation parameter.

3. RESULTS

The average number of iterations needed for the automatic registration was 206±68, and average time to compete the registration was approximately 5.2minutes (1.16 seconds per iteration) on a Pentium 400 MHz computer.

3.1 Visual verification

All results including the misalignment test and the simulated defect test were visually inspected and the quality of the results was rated as "very good", "lower quality" and, "poor quality". Successful registration was defined as the registration for which the visual agreement was “very good”. Using such criteria, 121 out of 125 studies misaligned within the range of 40° and 40 pixels were judged to be correctly registered. When quantified, all registrations visually judged as correct, converged with a variation in final transformation parameters of 0.75±0.35 pixels and 0.85±0.55°. The maximal difference from the mean for those registrations (qualitatively judged as correct) was 5.6 pixels (0.8mm) in X direction, 0.8 pixels (0.8mm) in Z direction and 6.8° in XY plane.

Figure 3 shows an example of registered datasets. The images include the realigned B-mode ultrasound images by using the transformation parameters obtained from the PD-MRA registration.

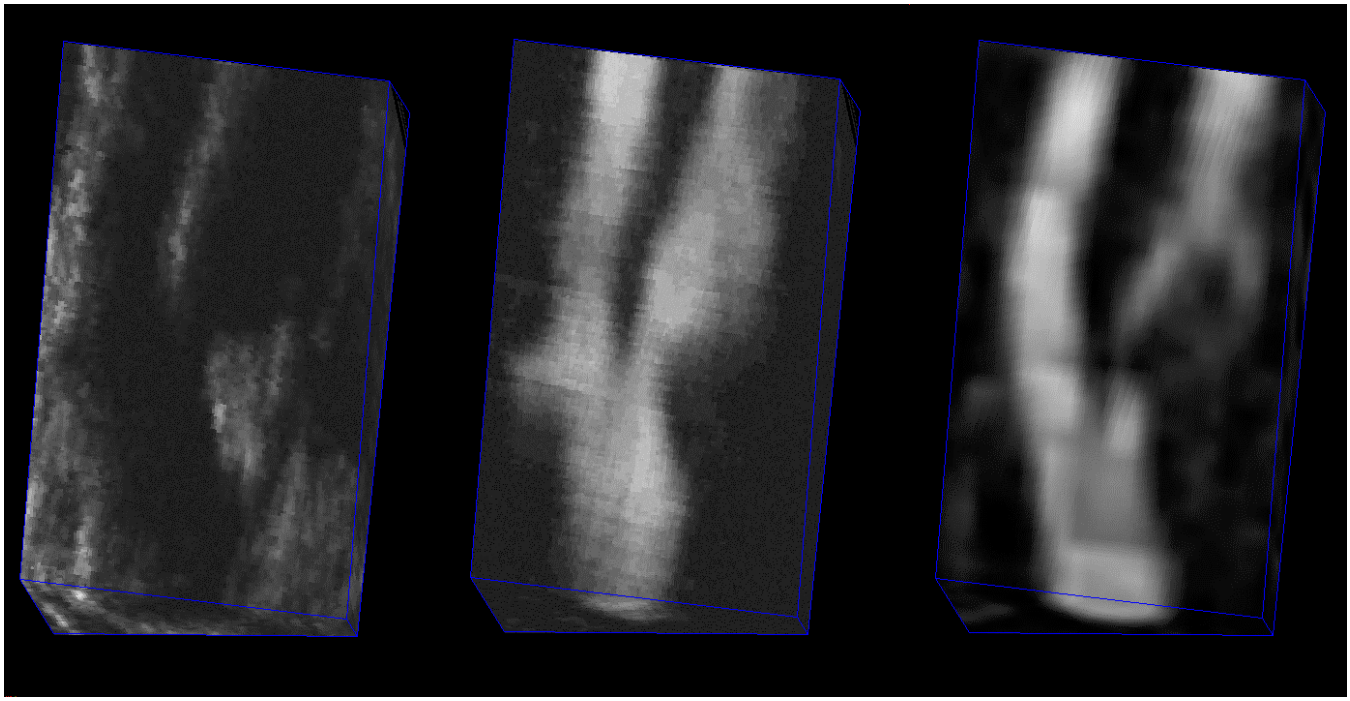

Figure 3. Co-registered B-mode (left), PD 3D (middle) ultrasound and MRA (right) images displayed in the same orientation.

3.2 Reproducibility

The mean total displacement registration errors (TDRE) due to the misalignment, calculated as described in eq 9 are shown in Figure 4. Misalignments larger than ≥ 50°, ≥50 pixels in the X,Y and ≥20pixels in the Z direction caused failure of the registration in 34 out of 60 test cases. In one patient study, the 20º YZ misalignment caused failure of the registration, this was due to the failure of the simplex algorithm which found a local minimum. These results are reflected in the values of the standard deviations of the errors presented in Figure 4. The mean and maximum total displacement errors for the range of 40° and 40 pixels in X, Y direction were below 5 pixels (0.8mm).

3.3 Simulated defect test

The effects on registration of simulated defects introduced on the Ultrasound images are presented in Figure 5. The SDRE error caused by the introduction of the simulated defects on the MRA images was 1.6±2.5°, 1.5±1.6 pixels in XY directions and 0.7±0.7 pixels in Z direction. Failures of registration occurred for one patient. In this case the field of view of the ultrasound was covering only the small portion of the internal and external artery. Consequently, the introduction of defects in either branch of the artery caused a large error in the XY angle, since information needed for determining the orientation along the long axis of the artery was missing. In all other cases, the registrations were judged as successful for the defects extending from 4 and 8 slices in all regions.

4. DISCUSSION

We have developed an automated technique for geometrically registering 3D MRA, 3D power Doppler, and 3D B-mode datasets of the diseased carotid bifurcation and tested it on selection of clinical patient data. The registration technique has the potential for both academic and clinical utility. The registered image pairs provide a common geometric framework in which to compare the two modalities quantitatively. In addition, the registered pairs allow one modality to compensate for the other's deficits. For example, the flow information lost in a turbulent MRA stenosis could be provided by the registered 3D Power Doppler.

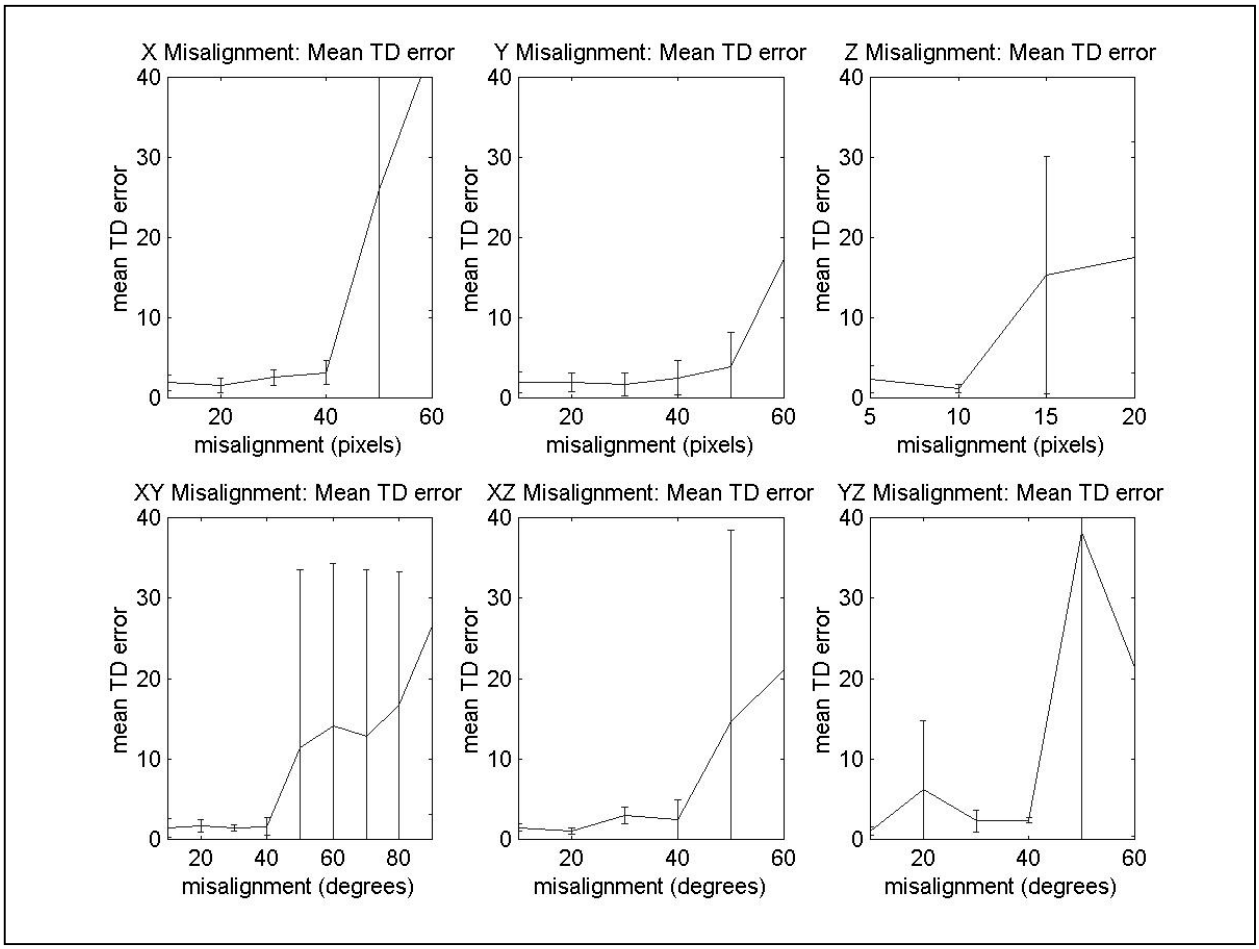

Figure 4. Mean and standard deviations of total displacement errors (TDRE) in the registration reproducibility test. Error units are in pixels for translations and in degrees for rotations.

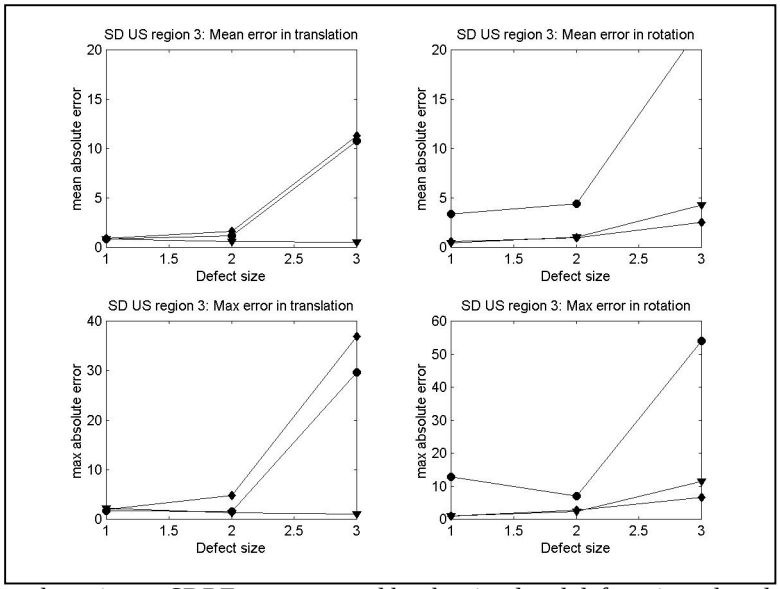

Figure 5. Mean (n=5) and maximum SDRE errors caused by the simulated defects introduced on ultrasound data in both arteries (region 3). Error units are in pixels for translations and in degrees for rotations. ● - X for translation, XY angle for rotation ◆- Y for translation, XZ angle for rotation ▼ - Z for translation, YZ angle for rotation

4.1 Registration algorithm.

The implemented algorithm is based on the Mutual Information[13] criterion derived from the combined multimodal image data-sets. This approach has been successfully applied in registration of brain images from various modalities[1-4,15]. Recently, it has been successfully applied to register serial ultrasound mammography images of the same patient in a semiautomatic manner[16]. Due to the large amount of noise present in ultrasound and MRA images of the carotid vessels, we had to threshold the images prior to the registration; this allowed the mutual information criterion to represent the measure of the alignment. Since the 3D ultrasound covered only a section of the MRA volume, we also needed to specify the approximate range of the field of view for the MRA images. This was typically not needed in previous applications of this criterion. Although threshold was selected specifically for the tested images, the same threshold was used for all test-cases. Apart from these pre-processing steps, the registration was fully automated. In spite of large differences in the coverage of the field of view and the noisy character of the data, the algorithm was in general very successful. The few failures were associated with finding the local minima rather than with an inappropriate value of the mutual information. This demonstrates the universal character of the mutual information approach, which is not specifically tailored for particular image features as many previous registration algorithms[4]

The successful performance of the algorithm is likely due to the fact that the data used in the registration were of similar nature; both PD US and the MRA are depicting the lumen of the vessels. We were not able to register automatically the B-mode data (which depicts plaque) to the MRA. However, since the B-mode data were acquired simultaneously with the PD we could indirectly place the B-mode in the MRA spatial orientation (Figure 3). The Ultrasound B-mode fusion with MRA is potentially of greater interest since plaque is not shown on MRA, but arguably MRA could provide better anatomical detail, or larger extent of the vessel than the Power Doppler.

An important application of the proposed registration technique would be to validate and compare the PD ultrasound technique for the automatic determination of the lumen size, in order to objectively evaluate the degree of stenosis[17]. The quantitative algorithms can be aided by the spatial coherence of the MRA and the PD data and the quantitative comparison on a voxel level could be performed. Such comparison should also include other modalities such as 3D rotational angiography [18]. Furthermore, a link between plaque and stenosis could be explored in detail in a similar voxel-by-voxel fashion. Ultimately, a full 3D-quantitifcation of the vessel stenosis and amount of plaque could be performed by an unsupervised computer program, from one or several imaging modalities.

The employed minimization algorithm is based on the simplex technique. This technique does not require the calculation of gradients at each evaluation unlike other minimization algorithms and has been shown to perform robustly for several image registration applications[7,19]. Further improvement of the simplex minimization should include the multi-resolution approach where sub-sampled 3D images are first registered to an approximate solution and then the registration is repeated allowing smaller range at higher resolution. The results of the misalignment tests suggest that in the range of the 40°, 40 pixels in X, Y direction and up to 15 pixels in Z direction the registration was successful. This range corresponds approximately to the 15 % of the field of view. An initial alignment within such range, could be accomplished by prior steps of the multi-resolution approach[2]. In order to preserve the sharp edges of the ultrasound at the lower matrix size selective data sampling could be used instead of the trilinear interpolation. Other types of initial alignment based on geometrical approaches such as principal axis method are likely to fail due to the differences in the field of view.[20]

Since the initial orientation of the raw images varied up to 180º in the case of the ultrasound data, it needed to be brought to the similar orientation and position to that of MRA before the registration. In practical clinical use, such rough initial alignment to an approximate position could be accomplished interactively in a very short time and subsequently the image could be registered with the use of our algorithm. Alternatively, standard orientation of the ultrasound acquisitions could be recorded with the data and this could be used as an additional information for the registration algorithm, providing an initial estimate. The approximate orientation could be also derived from the calibrated BIRD device[21].

4.2 Evaluation of the registration

We evaluated the reproducibility and the stability of the MRA-US registration technique by measuring the effects of the initial data misalignment and the effects of missing portions of the data on the registration parameters. Although we do not have the exact "gold standard" for the image position, these simulation tests allow us to estimate the performance of the algorithm on real patient data. The key difficulty in registering the clinical images is the variation in the anatomy and physiology. A phantom validation of the image-based registration technique, even with realistic design[22], would fail to

account for an unpredictable appearance of the data. By using several clinical datasets and performing simulated variation of the data (simulated defects) we are testing the algorithm in realistic conditions likely to be encountered in clinical practice.

The evaluation of the algorithm exposed some limitations of the proposed registration approach. Portions of both internal and external carotid arteries need to be present for the registration to succeed. Without this information the determination of the XY angle may not be correct. In the case of one patient we observed a distortion close to the bottom of the common carotid, despite the image registration and alignment in other parts of the vessels. This could be due to the vessel deformation between 2 procedures or due to image artifacts[23,24]. The 6-parameter search employed in this study does not compensate for such distortions. Other techniques such as deformable model approach[25] could be used to bring the data into improved alignment. These techniques should be applied after rigid-body alignment since only small deformations would likely be needed in such cases. The future use of the registration algorithm could be to quantify such non-linear distortions of the vessels. An additional modality useful in such comparison would be the 3D rotational angiography developed in our laboratory[18], which would provide high resolution, undistorted anatomical model.

The traditional methods of testing the accuracy of the registration algorithms employ the external fiducial landmarks as a "gold standard". Such markers provide the reference for the image-based registration. This approach was often followed in the validation of multimodality registration of brain scans[26]. However, in the case of carotid images, the locations of the arteries may not correspond to the external skin landmarks, due to the non-rigid character of the surrounding tissue. In addition, the need for the physical contact of the ultrasound probe with the skin would interfere with the external markers. The hypothetical possibility would be to use some kind of internal markers, if traditional angiography was performed. Such approach would need to be highly invasive and could still be potentially associated with significant errors, due to various image artifacts. Another possibility would be some kind of video-based system, where landmarks are determined optically, as used in some image guided surgery applications[27,28]. The optical system would not need to interfere with the ultrasound procedure. Such solution, however, would be associated with errors due to the skin deformations during the ultrasound scan and may not be practical since the clear optical path between the patient and the camera would be required.

REFERENCES

1. W. M. Wells, P. Viola, H. Atsumi, et al. "Multi-modal volume registration by maximization of mutual information," *Med. Image. Anal.* **1**, pp. 35-51, 1996.
2. C. Studholme, D. L. Hill, D. J. Hawkes. "Automated three-dimensional registration of magnetic resonance and positron emission tomography brain images by multiresolution optimization of voxel similarity measures," *Med Phys* **24**, pp. 25-35, 1997.
3. F. Maes, A. Collignon, D. Vandermeulen, et al. "Multimodality image registration by maximization of mutual information," *IEEE Trans Med Imaging* **16**, pp. 187-198, 1997.
4. J. West, J. M. Fitzpatrick, M. Y. Wang, et al. "Comparison and evaluation of retrospective intermodality brain image registration techniques," *J Comput. Assist. Tomogr.* **21**, pp. 554-566, 1997.
5. A. Savi, M. C. Gilardi, G. Rizzo, et al. "Spatial registration of echocardiographic and positron emission tomographic heart studies," *Eur J Nucl Med* **22**, pp. 243-247, 1995.
6. M. C. Gilardi, G. Rizzo, A. Savi, et al. "Registration of multi-modal biomedical images of the heart," *Q. J Nucl Med* **40**, pp. 142-150, 1996.
7. D. Dey, P. J. Slomka, L. J. Hahn, et al. "Automatic three-dimensional multimodality registration using radionuclide transmission CT attenuation maps: a phantom study," *J Nucl Med* **40**, pp. 448-455, 1999.
8. S. C. Strother, J. R. Anderson, X. L. Xu, et al. "Quantitative comparisons of image registration techniques based on high- resolution MRI of the brain," *J. Comput. Assist. Tomogr.* **18**, pp. 954-962, 1994.
9. D. D. Blatter. "Cerebral MR angiography with multiple overlapping thin slab acquisition. Part I. Quantitative analysis of vessel visibility," *Radiology*. **179**, pp. 805-811, 1991.
10. A. Fenster, D. Lee, S. Sherebrin, et al. "Three-dimensional ultrasound imaging of the vasculature," *Ultrasonics.* **36**, pp. 629-633, 1998.
11. D. B. Downey, A. Fenster. "Vascular imaging with a three-dimensional power Doppler system," *AJR. Am. J Roentgenol.* **165**, pp. 665-668, 1995.
12. W. H. Press, S. A. Teukolsky, W. T. Vetterling, et al. *Numerical Recipes in C*, Cambridge University Press, New York NY, 1992.
13. F. M. Reza. *An Introduction to the Information Theory*, Dover Publications Inc. New York, 1994.

14. P. Lacroute, M. Levoy. "Fast volume Rendering Using a Shear-Warp Factorization of the Viewing Transformation," *SIGGRAPH '94 Proceedings* pp. 451-458, 1994.
15. D. J. Hawkes. "Algorithms for radiological image registration and their clinical application," *J Anat.* **193**, pp. 347-361, 1998.
16. C. R. Meyer, J. L. Boes, B. Kim, et al. "Semiautomatic registration of volumetric ultrasound scans," *Ultrasound. Med Biol* **25**, pp. 339-347, 1999.
17. M. Eliasziw, R. F. Smith, N. Singh, et al. "Further comments on the measurement of carotid stenosis from angiograms. North American Symptomatic Carotid Endarterectomy Trial (NASCET) Group," *Stroke* **25**, pp. 2445-2449, 1994.
18. R. Fahrig, A. J. Fox, S. Lownie, et al. "Use of a C-arm system to generate true three-dimensional computed rotational angiograms: preliminary in vitro and in vivo results," *AJNR. Am. J Neuroradiol.* **18**, pp. 1507-1514, 1997.
19. P. J. Slomka, G. A. Hurwitz, J. Stephenson, et al. "Automated alignment and sizing of myocardial stress and rest scans to three-dimensional normal templates using an image registration algorithm" *J Nucl Med* **36**, pp. 1115-1122, 1995.
20. D. A. Weber, M. Ivanovic. "Correlative image registration," *Semin Nucl Med* **24**, pp. 311-323, 1994.
21. N. Hata, T. Dohi, H. Iseki, et al. "Development of a frameless and armless stereotactic neuronavigation system with ultrasonographic registration," *Neurosurgery* **41**, pp. 608-613, 1997.
22. W. Dabrowski, J. Dunmore-Buyze, R. N. Rankin, et al. "A real vessel phantom for imaging experimentation," *Med Phys* **24**, pp. 687-693, 1997.
23. C. R. J. Maurer, G. B. Aboutanos, B. M. Dawant, et al. "Effect of geometrical distortion correction in MR on image registration accuracy," *J Comput. Assist. Tomogr.* **20**, pp. 666-679, 1996.
24. R. Frayne, L. M. Gowman, D. W. Rickey, et al. "A geometrically accurate vascular phantom for comparative studies of x- ray, ultrasound, and magnetic resonance vascular imaging: construction and geometrical verification," *Med Phys* **20**, pp. 415-425, 1993.
25. A. F. Frangi, W. J. Niessen, R. M. Hoogeveen, et al. "Model-based quantitation of 3-D magnetic resonance angiographic images" *IEEE Trans. Med. Imaging* **18**, pp. 946-956, 1999.
26. R. P. Woods, S. T. Grafton, J. D. Watson, et al. "Automated image registration: II. Intersubject validation of linear and nonlinear models," *J Comput. Assist. Tomogr.* **22**, pp. 153-165, 1998.
27. K. Schwenzer, C. Holberg, J. Willer, et al. "3-D imaging of the facial surface by topometry using projected white light strips " *Mund. Kiefer. Gesichtschir.* **2 Suppl 1**, p. S130-S134, 1998.
28. P. L. Gleason, R. Kikinis, D. Altobelli, et al. "Video registration virtual reality for nonlinkage stereotactic surgery," *Stereotact. Funct. Neurosurg.* **63**, pp. 139-143, 1994.